Multiscale Science and Engineering (2022) 4:161–178
https://doi.org/10.1007/s42493-022-00086-9

REVIEW

Classical, Coarse-Grained, and Reactive Molecular Dynamics Simulations on Polymer Nanocomposites

Inseok Jeon[1] · Taeyoung Yun[2] · Seunghwa Yang[1]

Received: 1 August 2022 / Revised: 7 September 2022 / Accepted: 12 September 2022 / Published online: 22 September 2022

Abstract

Polymer-based nanocomposites have been one of the most spotlighted multifunctional condensed materials with the rapidly growing advancement of nanotechnology. Owing to the successful synthesis, manufacture, and characterization of various low-dimensional organic/inorganic nanoparticles and nanocarbon materials, it was expected that unprecedented excellent properties of composites can be achieved. However, disappointing results of the properties of newly designed nanocomposites, yet revealed structure-to-property relationship, and the limitations of the existing theoretical predictive models led to the exploration of new in silico simulation and review of micromechanics models. From the early 2000s, molecular dynamics (MD) simulation studies revealed the physics behind the unpredictable properties and microstructural evolution, such as the size-dependent properties, polymer sheathing, intrinsically weak adhesion between nanocarbon and polymer, and dispersion and agglomeration of fillers. The comprehension of the importance and impact of interface and interphase zone in nanocomposites enabled by the application of MD simulation led to revisiting composite micromechanics and the development of "interface/interphase models." In this review, the history of the successful application of classical, coarse-grained, and recent reactive MD simulations to the multifunctional properties of nanocomposites is retraced.

Keywords Polymer nanocomposites · Classical molecular dynamics · Coarse-grained molecular dynamics · Reactive molecular dynamics

Introduction

In 1989, Vollenberg and Heikens reported the first experimental observation of the filler size-dependent Young's modulus of nanocomposites. [1, 2]. Two years later Iijima reported the discovery of carbon nanotubes (CNTs), leading to the fourth-generation nanocarbon era [3]. Ajayan successfully aligned CNTs in a polymer matrix, leading to the era of "polymer nanocomposites" [4]. Ding et al. [5] demonstrated the polymer sheath around a multi-walled carbon nanotube (MWCNT) from the fracture surface of composites and supported the substantial interaction between MWCNT and engineering polymer. All these works are supported by sophisticated experiments. Wei et al. [6] observed the formation of a discrete adsorption layer corresponding to the polymer sheath around the MWCNT and further discussed the crystalline ordering of the molecules around the CNT using all-atom classical molecular dynamics (AACMD) simulation. The presence of the same highly densified and structurally ordered layer around spherical nanoparticles was revealed by MD simulations [7–9]. Naturally, materials scientists' efforts to take full advantage of the interphase zone and mechanists' endeavor to establish a structure–property relationship of nanocomposites including the "interphase" zone have been the main research areas in the field of multifunctional nanocomposites.

Meanwhile, some intrinsic disadvantageous features have been pointed out by extreme-scale computer simulations. For instance, nitrogen and oxygen atoms constituting typical engineering polymers are difficult to adhere to the surface of hexagonal carbon in CNTs unless external work is supplied [10]. To understand the substantial adhesion characteristics at the interface between nanofillers and

✉ Seunghwa Yang
fafala@cau.ac.kr

[1] Mechanical Engineering Division, School of Energy Systems Engineering, Chung-Ang University, 84 Heukseok-Ro, Dongjak-Gu, Seoul 06974, South Korea

[2] Korea Institute of Civil Engineering and Building Technology, 283 Goyangdae-Ro, Ilsanseo-Gu, Goyang-Si, Gyeonggi-Do 10223, South Korea

polymer matrix, the in silico pull-out test of 1-D nanocarbon structure has been effectively used. For instance, pull-out of a CNT from an epoxy matrix requires an interfacial shear strength of 61 MPa [11], whereas pull-out from a polyethylene (PE) matrix only requires 30 MPa of shear stress [12]. Even though interfacial shear strength it self does not completely indicate how effectively the interface between CNT and matrix can transfer the shear stress, the pull-out test with surface functionalization of CNT can qualitatively evaluate the weak nature of the interface between CNT and engineering polymer. For instance, the interfacial shear strength between a CNT and poly(methyl methacrylate) (PMMA) can be tailored by the phenyl functionalization of nanotubes [13]. Later, the transversely isotropic elastic stiffness of CNT/Polypropylene (PP) nanocomposites studied by sophisticated tensile simulation quantitatively confirmed that the intrinsically weak interface between CNT and PP can significantly degrade the shear modulus [14]. Since the mid-2000s, "interface/interphase" has been the most representative terminology in nanocomposites and is the focus of both materials scientists and mechanists, especially in the field of modeling and simulations [15].

Besides the interface/interphase, the agglomeration of embedded nanofillers has been a challenge to manifest efficient load transfer from the polymer matrix to the reinforcement by maximizing the contact area at the interface [16–19]. To understand the insufficient interpenetration of polymers into the gallery zone between individual fillers, modeling of poly-dispersed nanocomposites is required. Therefore, AACMD simulations are still limited despite the current computing capability of university laboratory-level parallel clusters. For instance, construction of single particle/amorphous polymer nanocomposites unit cell at dilute condition requires ~ 20,000 atoms, thus, poly-dispersed unit cell to consider particle agglomerations requires more than ~ 200,000 atoms with a complicated description of intramolecular interactions over 5 ns. Therefore, AACMD simulation has been extending the hardware limits until now. As an alternative, N-scale homogenization has been effectively used to establish agglomerated microstructure for macroscopic degradation of nanocomposites. Nonetheless, discrete modeling of insufficient permeation at the agglomerated interface is required to provide nanoscale information for microscale analysis. In this respect, coarse-grained molecular dynamics (CGMD) has been the focus area to narrow the gap between nanoscale and microscale [20–22].

In addition to the up-scaling issues of MD simulations, to account for the agglomeration and waviness of fillers in nanocomposites, recent studies are aimed at describing the detailed chemistry in matrix, filler, and interface. For instance, brittle failure of epoxy resin in nanocomposites involves the cleavage of the cross-linked network, which cannot be described through the classical potential models of covalent bonds using harmonic functions [23]. Owing to the development of ReaxFF adopting the bond order between a pair of atoms by interatomic distances [24], a more sophisticated and realistic description of local events in nanocomposites such as polymerization of epoxy molecules around the embedded CNT in nanocomposites [25] is now feasible. A breakthrough in simulating reactive phenomena such as the oxidation of polymers in the chemical aging process [26] and pyrolysis of thermoprotective polymers has expanded the horizon of MD simulations to predict the durability of nanocomposites under continuous exposure to ordinary as well as extremely harsh service conditions [27]. Compared with the classical MD simulations, however, evaluation of the bond order in implementing reaxFF-based MD simulation requires heavier computation time. Thus, the application of reactive molecular dynamics (RMD) simulation is restricted to smaller all-atom structures than in AACMD and CGMD simulations.

In retrospect, RMD, AACMD, and CGMD constitute a hierarchy of virtual experiments across spatial and temporal scales, as shown in Fig. 1. However, the maximum spatial scale available in CGMD simulation is restricted to 1000 nm. Therefore, sequential bridging to mesoscale and fully continuum scale computation theory is attempted to design multifunctionality of the nanocomposites. This semi-review briefly discusses the early-time efforts to establish valuable structure-to-property relationships of nanocomposites based on the AACMD simulation as well as the current attempts to narrow the gap between quantum mechanics and AACMD and between AACMD and micromechanics using the RMD and CGMD simulations, respectively.

Classical MD Simulation

The AACMD simulation commonly refers to a series of unit cell construction, geometry optimization, and thermodynamic ensemble simulation followed by a target production run using ordinary classical interatomic potential models without the consideration of bond order change. The classical potential models describe the behavior of primarily bonded backbones in typical engineering polymers through valence potentials including bond-stretching, angle-bending, bond rotation (torsion), and out-of-plane terms. In addition, short-range van der Waals (vdW) interaction and long-range Coulomb interaction are added to describe the secondary bonds in the system. Representative classical interatomic potential models include COMPASS, PCFF, CVFF, Amber, CHARMM, OPLS, Dreiding, UFF etc. For most linear and networked engineering polymers based on the hydrocarbon backbone and nanocarbons such as graphene with sp^2 resonant structure, these models provide valence and vdW potential parameters. For ceramics or minerals with more

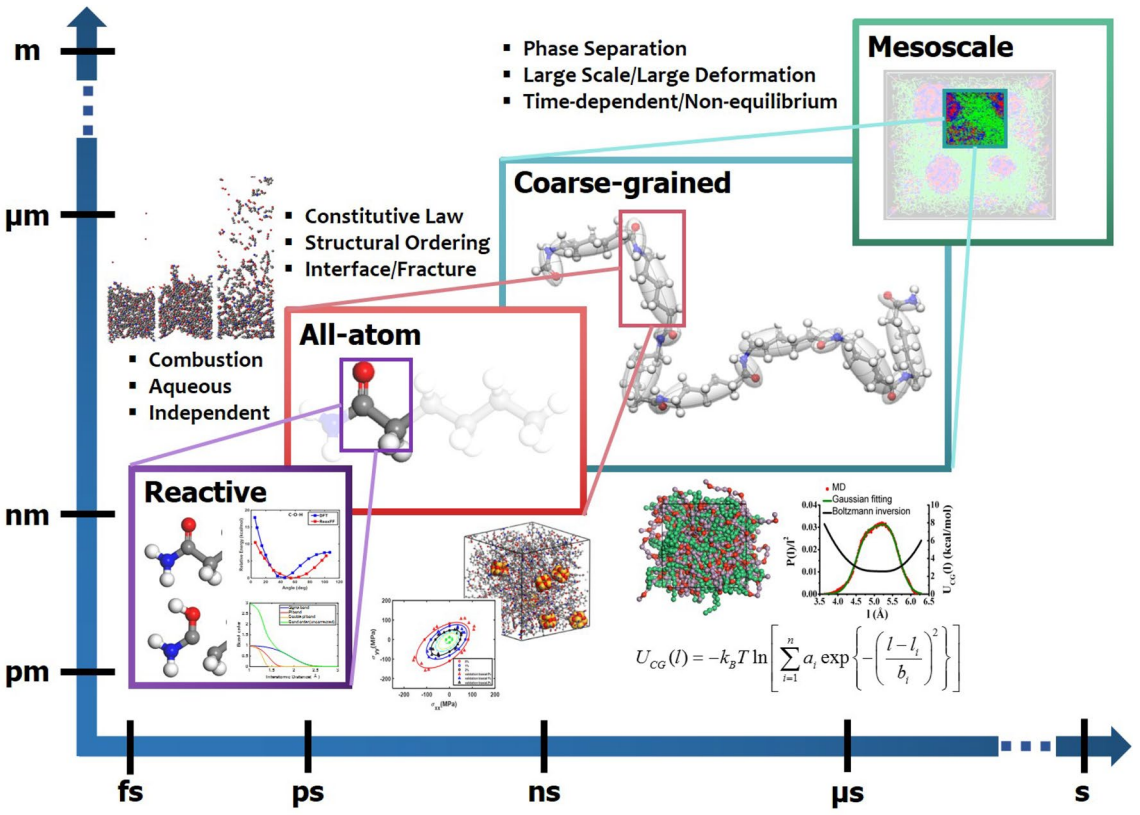

Fig. 1 Spatial and temporal scale of reactive, classical, and coarse-grained molecular dynamics simulations for condensed matter

complicated symmetry used for the nanoparticles and nanoclay, these potential models can describe the many-body effect to some degree. Depending on the combinations of the materials and the accuracy of the existing potential models, a cross combination of parameters has also been preferred. Most valence potential parameters are now accessible to academia as well as industry.

The classical potential models played a very important role in estimating the effective physical properties of thermoplastic-based nanocomposites such as elastic modulus [6, 7, 14, 19, 28–31], stress–strain curves [6, 28–30], thermal conductivity [32–36], thermal expansion, and glass transition behavior [37–39]. In most AACMD simulations, a unit cell of nanocomposites is constructed either by embedding one or several particles inside an amorphous polymer. For the 1D and 2D nanofillers such as CNT and graphene, fillers are fully embedded or partially embedded with infinite periodicity along one or two coordinate axes. Figure 2(a) and (c) show the front view of representative volume element molecular models of finite fully embedded CNT/PE nanocomposites [6] and infinitely periodic CNT-reinforced polyethylene terephthalate (PET) nanocomposites [29]. With a finite CNT, a clear improvement in the stress–strain behavior of PE curves could be achieved according to the longitudinal tension test, as shown in Fig. 2(b). The Young's modulus of nanocomposites determined from the MD simulation was underestimated compared with the Halpin–Tsai model prediction. For the infinitely long and covalently grafted CNT-reinforced nanocomposites, a clear withness of the discrepancy between MD simulation and Halpin–Tsai model prediction could be confirmed: the interface between pristine CNT and engineering polymer is weak, as shown in the transverse tension [Fig. 2(e)] and longitudinal shearing [Fig. 2(f)]. Before the intrinsic weak interface was confirmed from MD simulations [14], equivalent constitutive models for the nanocomposites were mostly focused on the description of the interphase zone with a perfect interface condition.

In addition to the stress–strain behavior and elastic moduli, research on revealing the abnormal structural conformation of matrix molecules around nanoparticles was performed through the density distribution and orientation order functions. Linear polymers such as PE tend to form entropy-driven self-assembly around CNTs and graphene. The density and crystallinity of the self-assembled zone are characterized by the radial density distribution and orientation order parameter $S_Z(r) = 0.5\left[3\left\langle \cos^2(\theta)\right\rangle - 1\right]$, where θ is the angle between the reference axis such as the longitudinal direction of CNT and the vector defined to represent the direction of the small segment in the backbone, and r is the distance from the center of CNT in a unit cell to the centroid

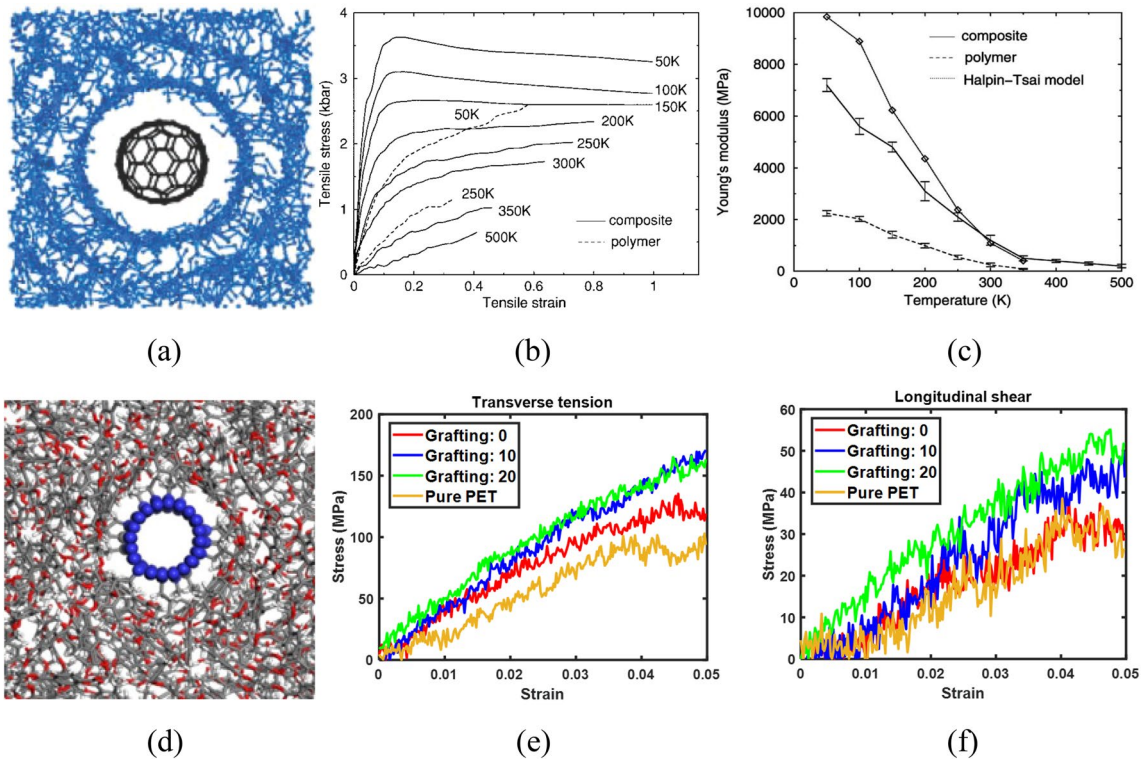

Fig. 2 Representative molecular unit cell modeling and mechanical behavior of SWNT/polymer nanocomposites. **a** Front view of capped SWNT in PE matrix **b** Temperature-dependent stress–strain curve of SWNT/PE nanocomposites under longitudinal tension **c** Comparison of the longitudinal Young's modulus of nanocomposites determined from MD simulation and Halpin–Tsai model [6] [Copyright (2008) American Chemical Society] and **d** Front-view of infinitely long CNT covalently grafted to PET matrix **e** Transverse strain-transverse stress curve **f** Longitudinal shear stress-shear stress curve [29] [Copyright (2022) Elsevier]

of the segment. As the backbone in the polymer becomes parallel to the axis of CNT, $S_z(r)$ increases. As shown in Fig. 3(a), both the radial density distribution and orientation order show periodically developed peaks around the CNT. The coincident peaks in Fig. 3(a) indicate that the interphase zone is highly densified than other matrix zones as well as aligned to the axial direction of CNTs. The radial density distribution of inorganic spherical particulate nanocomposites also shows a similar primary peak in the vicinity of the nanoparticles [7, 8]. Since the surface functionalization of nanoparticles readily influences the adhesion characteristics at the interface, the density of the interphase zone varies with the type of functional units or covalent grafting.

For inorganic nanoparticulate composites, the characterization of the interphase zone and the associated particle size-dependent properties were more attracting issues than the intrinsically weak interface in nanocarbon-based nanocomposites. As the size of the embedded nanoparticle becomes less than the radius of gyration of polymers in the matrix, the interphase zone becomes a critical factor. For instance, the elastic modulus and coefficient of thermal expansion (CTE) of nanocomposites embedding smaller nanoparticles show a better reinforcing effect than those with larger nanoparticles [7, 37, 42–45]. The size-dependent improvement in nanoparticulate composites can be simply elucidated by the relative volume fraction of the interphase zone according to the particle radius and superior properties of the interphase zone. In the thermal transport problem, however, the interface zone attracted more attention due to the phonon scattering and reflection at the interface. The phonon is a continuous flux of the vibrational motion of atoms in molecules; thus, phonon transfer through primary bonds is more efficient than through secondary bonds. Unless the interface is properly grafted or the surface of the particle is functionalized, finite thermal resistance always exists at the interface. Since the interface zone can be regarded as an additional phase with finite conductivity, the effect of the thermal resistance shows filler size dependency. Owing to the rivaling effect of the interphase and thermal resistance, the effective thermal conductivity of epoxy reinforced with silicon carbide (SiC) showed a critical particle radius to maximize the size effect of SiC nanoparticles [43]. Below the critical radius, the thermal conductivity of the composites could be even less than that of neat epoxy matrix.

While most early-time AACMD simulations considered defect-free nanofillers or designed surface functionalization,

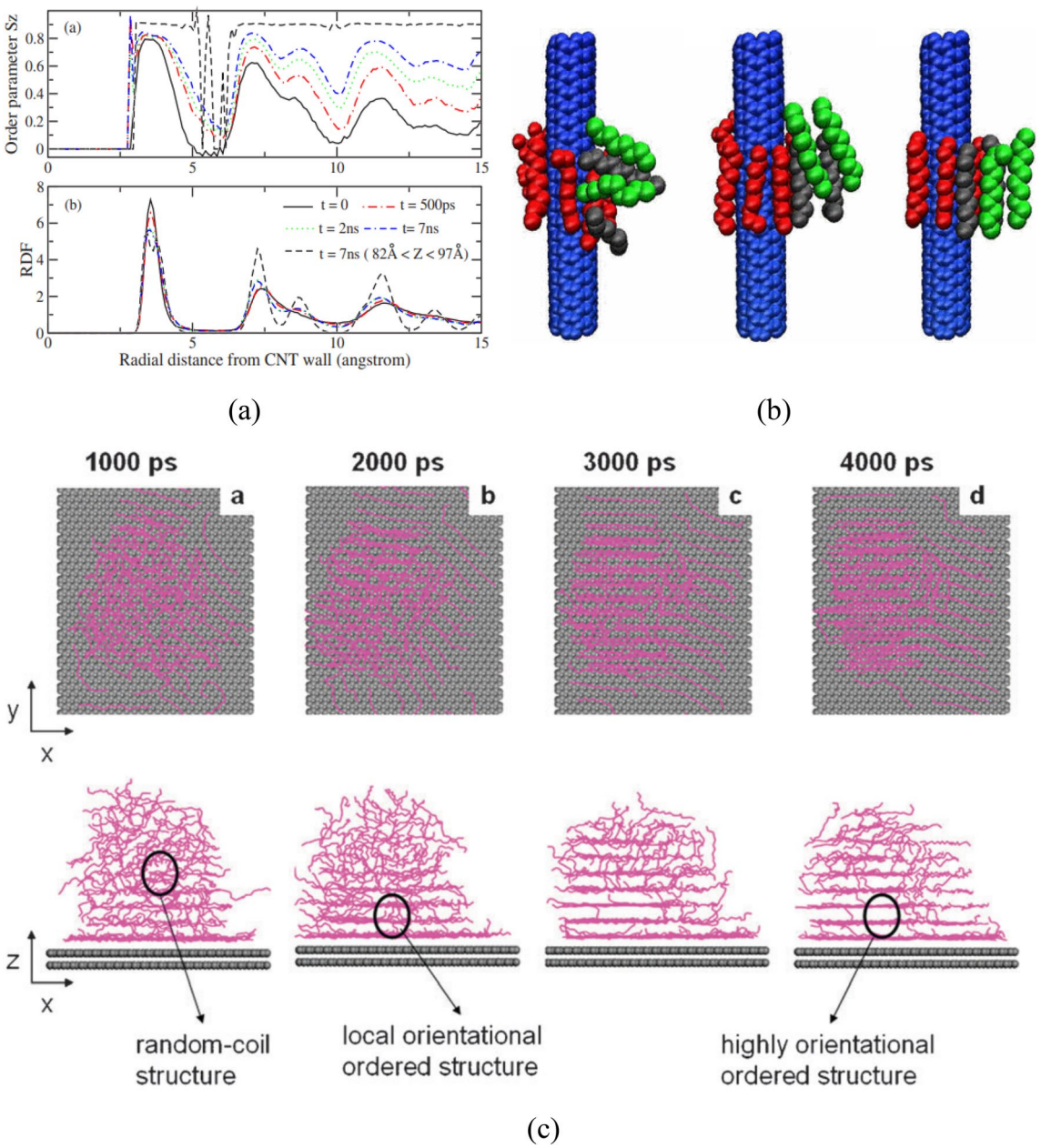

Fig. 3 **a** Orientation order parameter and radial density distribution of alkane molecules around (5,5) CNTs at various time during NVT ensemble simulation at 300 K for 7 ns **b** Change of alkane conformation at t = 0, t = 200 ps, and t = 300 ps (from left to right) [40] [Copyright (2007) American Physical Society] **c** Self-assembly and crystallization of random-coiled alkane molecules during the NVT ensemble simulation at 500 K [41] [Copyright (2011) Royal Society of Chemistry]

recent studies after the 2010s consider the inevitable and practical structural factors. For instance, CNTs in polymers are not defect-free. For inorganic nanoparticles such as silica, however, point defects are not an important factor since dislocation under mechanical behavior is difficult. For tubular structures or hexagonal nanosheets such as graphene, alteration of the electronic structure results in significant degradation [46]. For instance, the elastic stiffness of graphene is largely degraded by epoxide and hydroxyl functionalization, as shown in Table 1 [47]. In this respect, surface functionalization of the CNTs naturally bears hybridization of sp^2 structure in the sidewall. According to the micromechanics of composites, the degradation of nanocarbon results in the degradation of nanocomposite properties.

However, an interesting study on the positive aspect of the crystallographic defects in CNTs on elastic moduli of nanocomposites was reported by classical MD simulation. According to the transversely isotropic elastic modulus of

Table 1 Elastic constants of graphene with various epoxide and hydroxyl groups [GPa] [47] [Copyright (2021) Elsevier]

	C_{22}	C_{23}	C_{33}	C_{32}	E_L	$C_{44}(=G_T)$
Pristine	1373	557	1360	565	1047	314
5 Epoxied	1176	362	1151	390	993	252
10 Epoxied	1002	147	875	221	944	196
15 Epoxied	937	141	818	189	887	204
5 Hydroxyl	1177	404	1200	385	1023	264
10 Hydroxyl	1127	310	1076	345	1006	274
15 Hydroxyl	956	186	904	181	964	222

nanocomposite unit cells reinforced by pristine and Thrower-Stone–Wales (TSW)-defected CNTs [48], the longitudinal elastic modulus of infinitely long CNT-reinforced nanocomposites decreases as the defect density in CNTs increases, as shown in Fig. 4(a–b). On the contrary, the transverse Young's modulus where the interfacial load transfer between CNTs and polymer matrix plays an important role increases even if the elasticity of the CNTs is degraded by the TSW defect as shown in Fig. 4(c). According to the CNT pull-out test embedding void, TSW defect and adatom defects using the PCFF force field, improved adhesion energy between the TSW-defected CNTs and polymer resulted in increased interfacial shear strength, as depicted in Fig. 4(d–e). For the TSW defect, however, the PCFF force field does not distinguish the carbon atoms in hexagon, pentagon, and heptagon since the TSW defect can sustain sp^2 hybridization. Therefore, a mechanism other than the adhesion was required to establish the structure–property relationship for the defect engineering of nanocomposites.

From AACMD simulation on TSW-defected and oxygen-functionalized graphene-polymer nanocomposites, the role of the surface roughness of graphene induced by the defect was studied in detail [47, 50, 51]. As shown in Table 2, the surface roughness of graphene increases by oxidation and TSW defect. To correlate the surface roughness and the interfacial shear load transfer, the evolution of shear stress in graphene and polymer matrix was analyzed in detail. As shown in Fig. 4(f), the shear stress in pristine graphene does not increase as the nanocomposite unit cell is sheared. On the contrary, the shear stress in hydroxyl-functionalized graphene and its surrounding matrix prominently increases and suddenly drops at the same strain applied to the nanocomposites. The results shown in Fig. 4(f–g) confirm the possibility of defect engineering that understanding and controlling the intrinsic defects can be better solutions than removing the defects to achieve a better reinforcing effect.

Coarse-Grained MD Simulation

The AACMD simulations applied to the polymer nanocomposites are limited to below hundreds of nanoseconds and nanometer scale simulations of periodic representative unit cell structures. However, several important properties of nanocomposites are attributable to the microscale structures and microseconds of time evolution, which are inaccessible by AACMD. To resolve the limitations and explore time-dependent behaviors such as viscoelasticity and rheology, poly-dispersed microstructural events such as particle agglomeration, and thermodynamics description of equilibrium such as phase dissolution and separation of complexes, CGMD simulations have been attempted. Until now, most of the above-mentioned time-consuming behaviors or large-scale events have been studied through a direct hierarchical scale bridging of AACMD simulations and continuum micromechanics.

In early-time CGMD studies, the motion of beads representing a group of atoms in the system was described using harmonic potential or stiff finite extensible nonlinear elastic potential (FENE) with LJ reduced units for energy coefficients. For the nanocomposites, embedded nanoparticles are represented by simple beads, and their interactions are described using LJ-type truncated and shifted potentials [20, 52–55]. The reduced parameter-based CGMD simulation was useful to understand the structure-to-property relationship of poly-dispersed nanocomposites unit cell structures. For instance, parametric studies on the effect of nanoparticle-polymer interaction strength, particle grafting to the polymer, particle agglomeration, and filler volume fractions on the mechanical behavior of filled polymers could be performed with ease for optimum design of composition and microstructures.

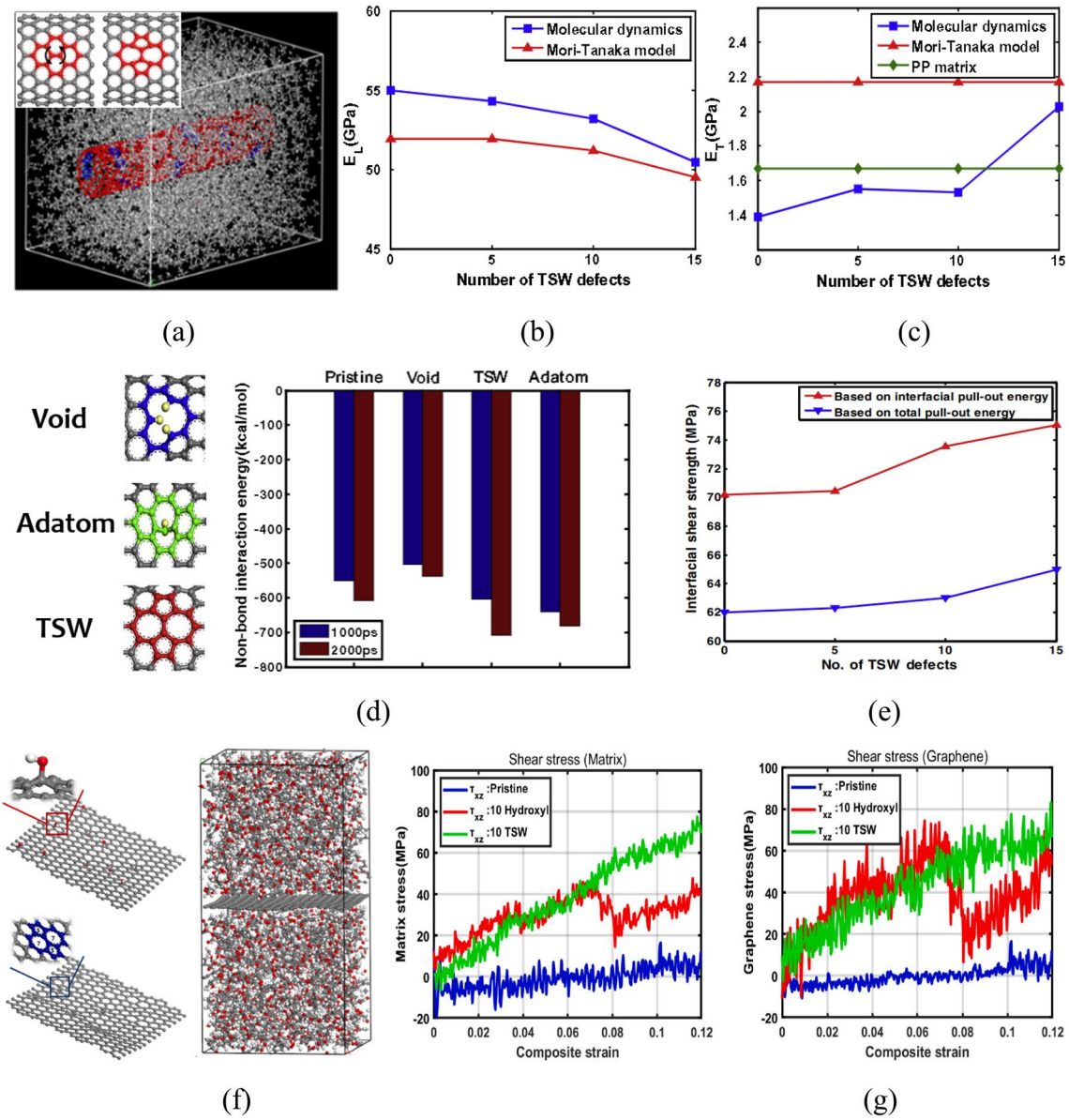

Fig. 4 **a** Transversely isotropic periodic unit cell of TSW defected PP nanocomposites **b** Longitudinal Young's modulus of nanocomposites **c** Transverse Young's modulus of nanocomposites [48] [Copyright (2013) Elsevier] **d** Adhesion energy between defected CNT and PP matrix **e** Interfacial shear strength between TSW defected CNT and PP matrix [49] [Copyright (2015) Elsevier] **f** Transversely isotropic periodic unit cell of graphene/PET nanocomposites **e** Shear stress in graphene and PET matrix during longitudinal shearing of nanocomposites model [51] [Copyright (2022) Elsevier]

Table 2 Arithmetic average roughness of graphenes [51] [Copyright (2022) Elsevier]

System	Roughness (Å)	Maximum displacement (Å)
Pristine graphene	0.41	1.32
Hydroxylated graphene	0.62	3.46
TSW defected graphene	0.74	2.09

Despite the advantages of applying CGMD simulations, there are certain limitations to taking full advantage of coarse-graining the polymer backbone to improve the computational efficiency. A group of atoms is mapped into a bead or superatom to represent the whole polymer matrix and inclusions using reduced degrees of freedom in CGMD. Therefore, a proper description of the interactions between the beads is critical to reproducing the structural conformations and predicting the target properties with accuracy in comparison with the AACMD. The parameterization of the

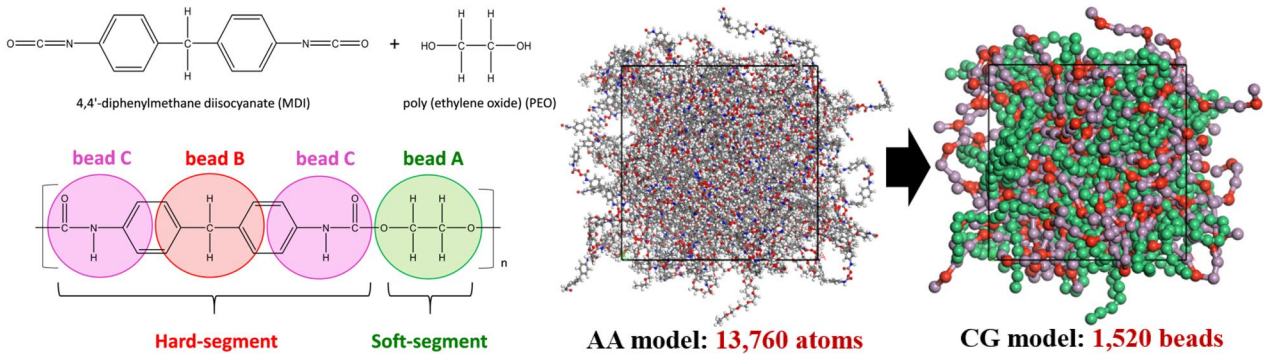
4,4'-diphenylmethane diisocyanate (MDI)
poly (ethylene oxide) (PEO)
bead C
bead B
bead C
bead A
Hard-segment
Soft-segment
AA model: 13,760 atoms
CG model: 1,520 beads

(a) (b)

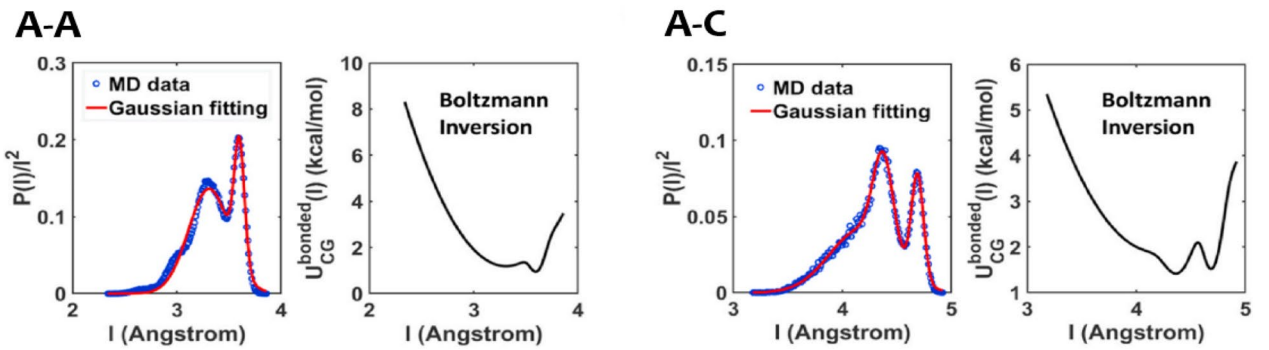
A-A
MD data
Gaussian fitting
P(l)/l²
l (Angstrom)
Boltzmann Inversion
U^bonded_CG(l) (kcal/mol)
A-C
MD data
Gaussian fitting
P(l)/l²
l (Angstrom)
Boltzmann Inversion
U^bonded_CG(l) (kcal/mol)

(c)

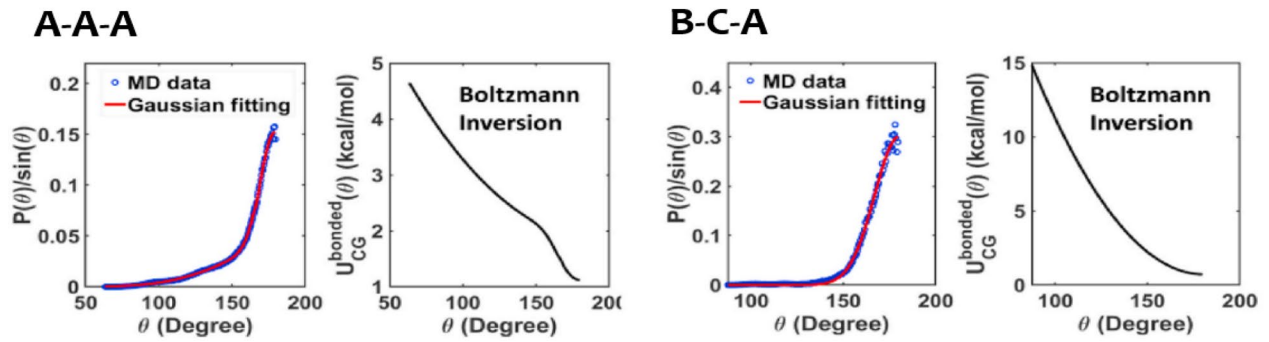
A-A-A
MD data
Gaussian fitting
P(θ)/sin(θ)
θ (Degree)
Boltzmann Inversion
U^bonded_CG(θ) (kcal/mol)
B-C-A
MD data
Gaussian fitting
P(θ)/sin(θ)
θ (Degree)
Boltzmann Inversion
U^bonded_CG(θ) (kcal/mol)

(d)

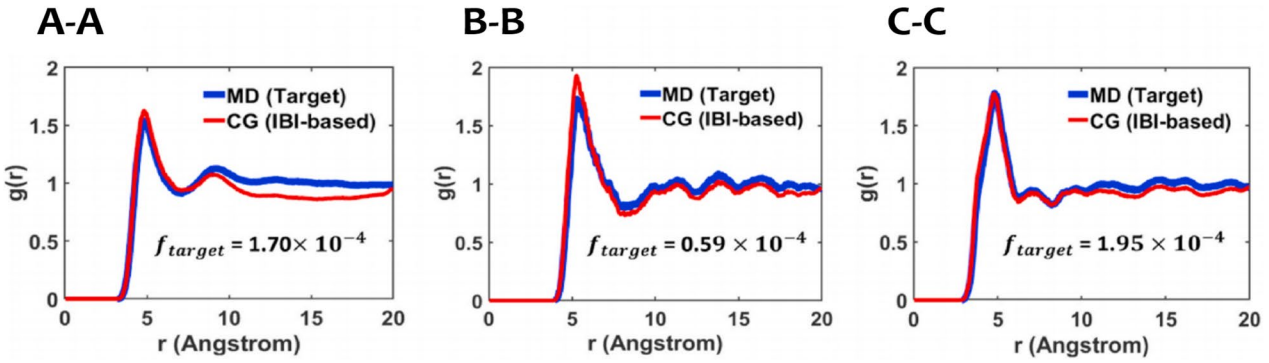
A-A
MD (Target)
CG (IBI-based)
g(r)
f_target = 1.70× 10⁻⁴
r (Angstrom)
B-B
MD (Target)
CG (IBI-based)
g(r)
f_target = 0.59 × 10⁻⁴
r (Angstrom)
C-C
MD (Target)
CG (IBI-based)
g(r)
f_target = 1.95 × 10⁻⁴
r (Angstrom)

(e)

◂**Fig. 5** **a** Mapping of AA model to super atoms **b** AA model and equivalent CG model for conformational matching **c** Bond length distribution and corresponding potential energy curve **d** Bending angle distribution and corresponding potential energy curve **e** RDF of AA and CG model [56] [Copyright (2021) Elsevier]

CG potential is dependent on several state- and material-based parameters such as the type of polymers and inclusions, properties to be determined, and temperatures. Recent efforts in the parameterization of CG potentials have been aimed at reproducing the thermomechanical properties of nanocomposites with accuracy.

The most representative parameterization method for real unit CGMD simulation is the Boltzmann Inversion (BI) and Iterative Boltzmann Inversion (IBI). The BI method starts from the definition of CG bead and matches the conformational distribution of CG and AA model to construct bonded parameters. For instance, the AA model of a shape memory copolymer consisting of 4,4′-diphenylmethane diisocyanate (MDI) and polyethylene oxide (PEO) can be represented by three beads, as shown in Fig. 5(a) [56]. Then, the bond length and bending angle defined in the CG model are chosen as a state in the Boltzmann distribution, and their distributions obtained from the current CG configuration are fitted into a simple harmonic or Gaussian distribution. For instance, the AA model of a shape memory copolymer consisting of 4,4′-diphenylmethane diisocyanate (MDI) and polyethylene oxide (PEO) can be represented by three beads, as shown in Fig. 5(a) [56]. Since the distribution of bond length and bending angle has multiple minima or arbitrary distribution, a multi-centered Gaussian distribution is occasionally used. Using Gaussian fitting, the bond-stretch and angle-bending potential parameters of beads A, B, and C are derived from BI method. Depending on the correlation between the MD data and Gaussian fitting in Fig. 5(c) and (d), additional iterations are used in the IBI method.

Once the bonded parameters are prepared, non-bonded CG parameters are derived. The radial distribution function (RDF) is defined as the probability of the system in Boltzmann distribution, and the IBI method is adopted for the parameterization. The solution process starts from the target RDF of the CG unit cell just mapped from the AA unit cell. Then, the first non-bond potential energy is determined from the first BI followed by the implementation of the first CGMD simulations. The RDF of the CG unit cell after its first implementation does not match the target RDF; thus, energy correction is defined using the target and first RDF. To evaluate the RDF matching, the target function is also defined to decide whether the iteration is continued or not. The non-bond potential energy is updated by adding the energy correction to the first energy, and the second round IB is implemented. After the convergence, the non-bond energy is finally corrected to accurately reproduce the density of the reference AA unit cell. The IB and IBI methods are focused on the matching of structural distributions of bond length, angle, and RDF; thus, it is not clear whether the bonded and non-bonded CG potential models can accurately reproduce the other thermomechanical properties of the original AA model [57, 58].

Against the intrinsic limitations of IBI, recent studies are providing additional parameter tuning processes of non-bonded potentials to reproduce stress–strain curves, thermal expansion coefficients, and glass transition temperatures [59]. For instance, the pressure correction process at a single temperature used in RDF-trained non-bonded CG potential does not guarantee the temperature transferability of the system density, as shown in Fig. 6(b). To decrease the difference between the CG model prediction and AA model reference density in a wide range of temperatures, the non-bonded energy coefficients σ and ε define the equilibrium distance between the beads and energy wall depth, respectively, according to the quadratic polynomial function $\sigma = aT^2 + bT + c$, where T is the temperature of the system. For the CG model of linear polystyrene shown in Fig. 6(a), such a temperature-dependent definition of the non-bonded energy could guarantee the temperature transferability in elastic modulus, as shown in Fig. 6(b). However, the temperature-dependent pressure correction results in discrepancies in RDF [59]. For more complicated polymers such as cross-linked epoxy, the non-bonded CG potential parameters are expressed in terms of the temperature as well as the degree of cross-linking (DOC). For the parameterization, advanced optimization such as artificial neural network (ANN)-assisted particle swarm optimization (PSO) is used to determine robust non-bonded potential parameters available at different temperatures and DOC, as shown in Fig. 6(c). For the machine-learning-assisted CG modeling, the temperature transferability at varying DOC in elastic modulus of cross-linked epoxy could be guaranteed, as shown in Fig. 6(d). To increase the versatility of the CG potential, however, additional thermoelastic properties should be obtained through AA models or experiments. Moreover, despite the effect of bonded potential in the mechanical behavior of linear as well as crosslinked polymers, only the non-bonded parameters have been continuously tackled and re-parameterized to fit the given AA simulation or experimental data.

The CGMD has been effectively used to study the time-dependent behavior of polymers and polymer nanocomposites such as creep [60], viscoelastic moduli [61, 62], interfacial damping, and energy dissipation under cyclic loading conditions [62, 63]. For the graphene-PMMA nanocomposites, the CG mapping could be constructed for both phases, as shown in Fig. 7(a). The CG parameters for graphene were determined by the strain energy matching technique, whereas the bonded and non-bonded parameters for the PMMA matrix were determined by the IB method. For the

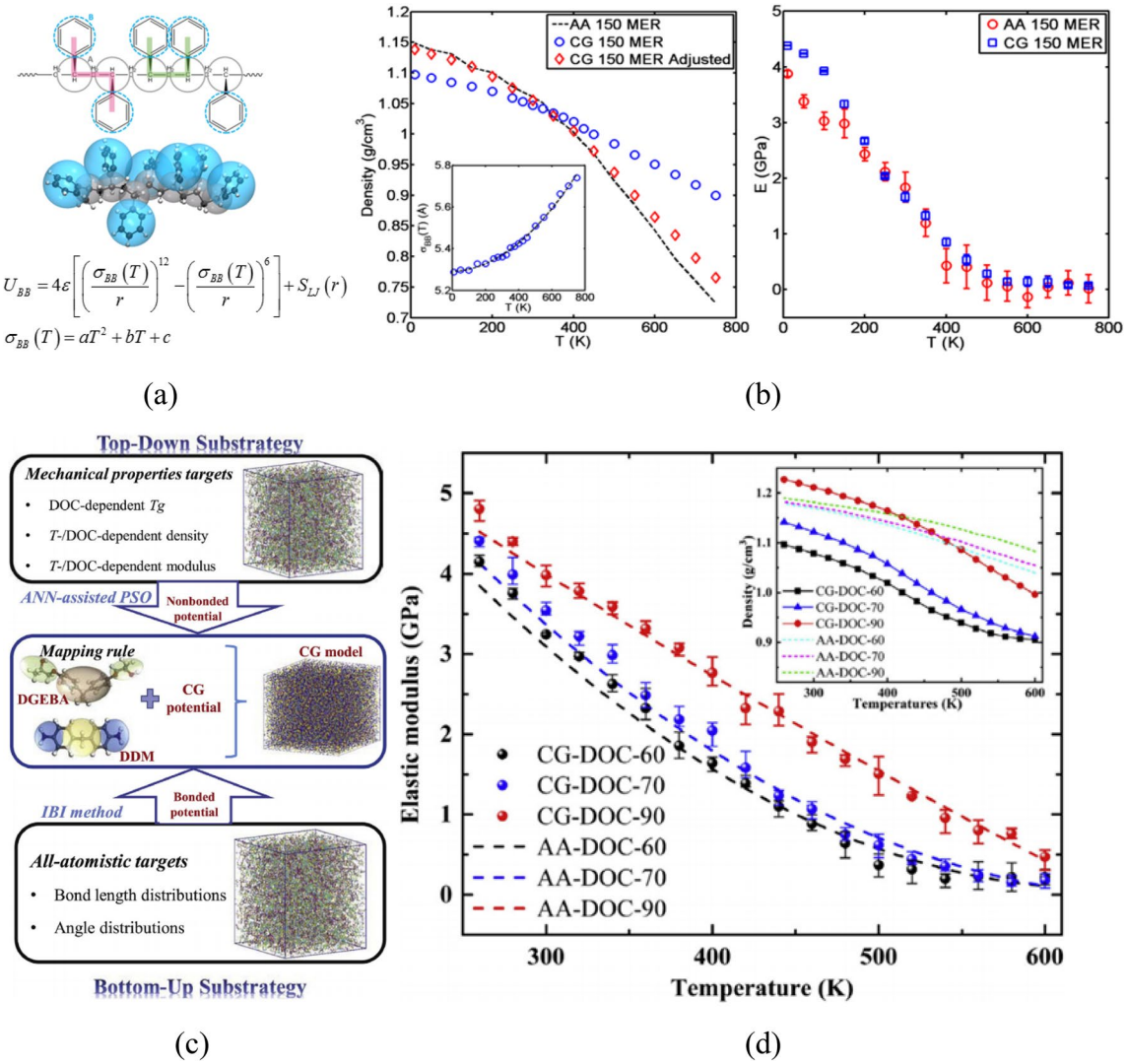

Fig. 6 **a** Mapping of polystyrene AA model to beads **b** Comparison of CG and AA density (left) and Young's modulus (right) after temperature-dependent density correction [59] [Copyright (2015) America Chemical Society]. **c** Schematic view of CG model parameterization for epoxy combining IBI and ANN-assisted particle swarm method **d** Temperature transferability of the elastic moduli obtained from CGMD in comparison with AA simulation result with varying DOC [58] [Copyright (2019) Elsevier]

transversely isotropic CG unit cell where finite three-layer graphite is embedded, a small amplitude oscillatory shear (SAOS) was imposed to study the mechanical and viscoelastic behavior of nanocomposites, as shown in Fig. 7(b). To account for the waviness of the embedded graphene layers, the geometry of the curved surface of graphene is described by a sinusoidal function $z = h\sin(2\pi x/l)$, where h is the amplitude of the wavy graphene, and l is the wavelength of the graphene embedded in the PMMA matrix, as shown in Fig. 7(b).

When the nanocomposite was exposed to the SAOS deformation, the sinusoidal strain resulted in a sinusoidal evolution of the internal shear stress $\tau = \tau_0 \sin(\omega t + \delta)$ with a finite phase lag of δ, as shown in Fig. 7(d). Thus, the storage modulus G' and loss modulus G'' of the nanocomposites can be calculated. From the phase lag, the loss tangent tan(δ) describing the material's damping characteristics can also be determined according to the frequency of SAOS. The dynamic moduli of graphene/PMMA nanocomposites are arranged in Table 3 according to the waviness of the embedded graphene. Compared with pure PMMA, all the nanocomposite unit cells show improved tan(δ), indicating that the embedded graphene increases the interfacial friction loss, thus improving the damping characteristics. Compared with flat graphene, wavy graphene shows better energy dissipation capability with a bit larger tan(δ). Specifically, when $l = 20$ nm, the nanocomposites show remarkably high energy dissipation performance in comparison with other

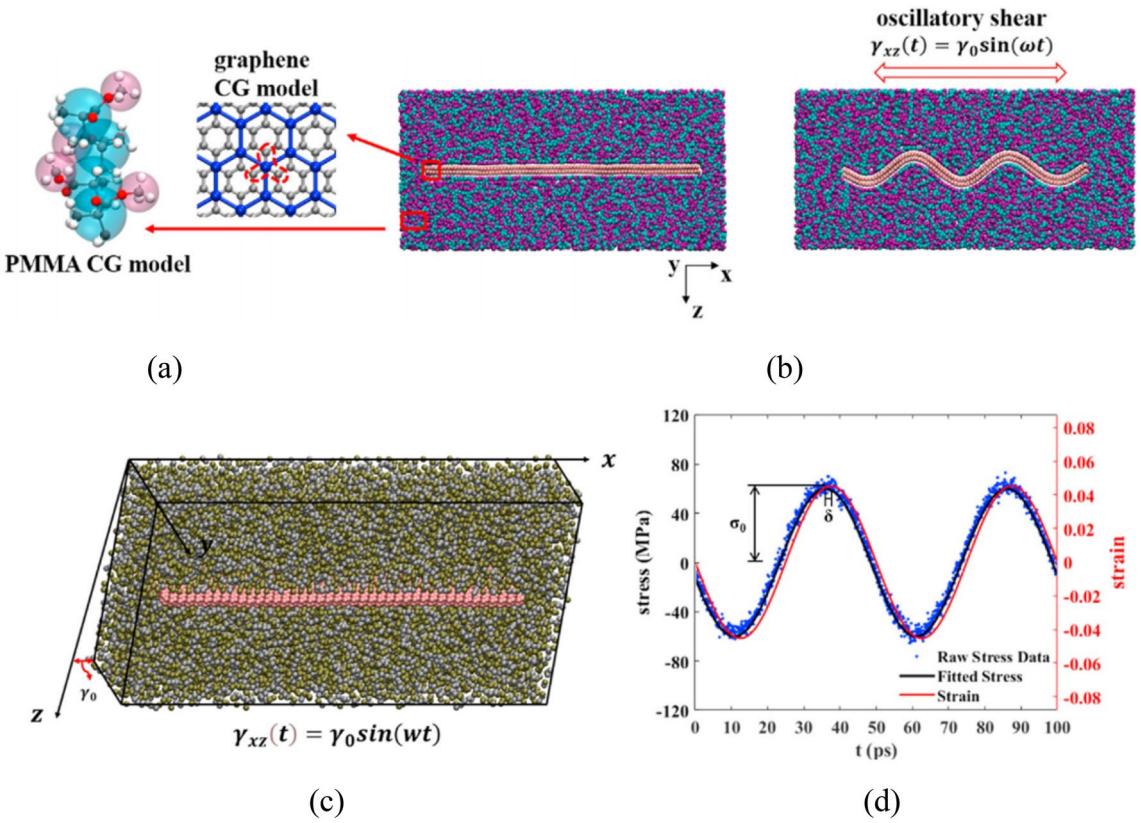

Fig. 7 **a** Mapping of PMMA and graphene AA model to beads **b** Nanocomposite unit cell loaded with straing (left) and wavy (right) graphene **c** SAOS simulation of nanocomposites **d** Represenative stress–strain relationship of nanocomposites during SAOS [62] [Copyright (2021) Elsevier]

Table 3 Dynamic moduli of nanocomposites reinforced by wrinkled bilayer graphene sheets and bulk PMMA [62] (Copyright 2021 Elsevier)

	Flat	l= 40 nm	l= 20 nm	l= 10 nm	l= 8 nm	PMMA
G' (MPa)	1097.3	1095.4	507.7	1132.7	1109.3	1311.2
G'' (MPa)	303.3	305.0	523.4	294.8	308.9	236.6
tan(δ)	0.276	0.279	1.031	0.260	0.279	0.181

wavy graphene forms. Thus, the CGMD simulation study of wavy graphene-reinforced nanocomposites can be useful for the design of damping performance at a specific frequency of SAOS. To obtain frequency-dependent damping characteristics, the SAOS requires a much longer time for calculating the phase lag between the applied strain and resultant stress. CGMD can provide useful time-dependent parametric studies, which were not accessible in AA simulations, in a wide timespan.

Reactive MD Simulation

Both AACMD and CGMD have enabled the prediction of various material properties of nanocomposites and structure–property relationships. Nonetheless, the gap between quantum mechanics simulation and AACMD simulation exists, and the applicability of AACMD is diminishing. For instance, no matter how high the temperature of the polymer unit cell is set, the backbones of polymer chains in the unit cell remain connected. Therefore, the response of the polymer at an elevated temperature is always disentanglement of individual chains in diffusion, and the thermal decomposition of polymers is not described. Moreover, classical potential simulations of copper nanoparticles in a water bath do not predict the dissociation of water followed by oxidation of copper atoms and desorption into the solvent. To materialize the reactive event from in silico simulations, quantum–classical molecular dynamics (QCMD) simulations based on density functional tight-binding (DFTB) simulations have been developed [64]. However, QCMD still limits the available system size and time scale to less than a thousand atoms

and several picoseconds, respectively. For hydrocarbon systems, reactive bond order potential (REBO) has been successfully applied to predict the properties of fillers such as graphene and polymers such as PE [65]. The REBO potential was not parameterized for various atoms and is limited to carbon, hydrogen, and oxygen.

Between the computational accuracy of ab initio simulation and the cost-effectiveness of classical MD simulation, reaxFF-based RMD simulation has been widely applied as a representative RMD simulation. As opposed to QCMD, reaxFF does not describe the electronic structure using DFT; however, it assumes that the bond order between paired

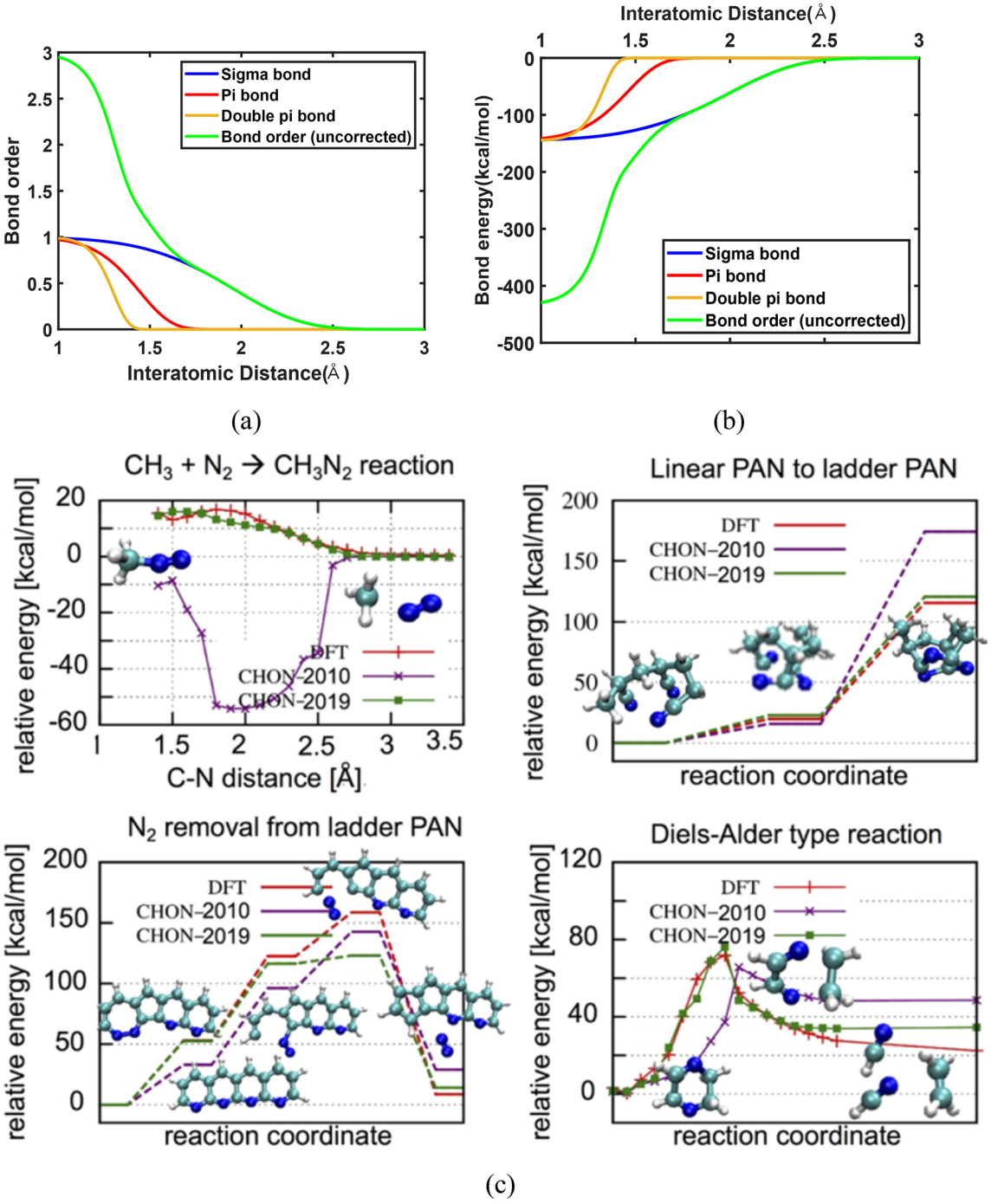

Fig. 8 **a** Interatomic distance-dependent bond order change of carbon–carbon bond and **b** Variation of bonding energy [24] [Copyright (2019) American Chemical Society]. **c** Comparison between DFT and ReaxFF for PAN related chemistry [66] [Copyright (2019) American Chemical Society]

atoms can be determined from the interatomic distance, as shown in Fig. 8(a) [24]. For instance, carbon–carbon pair can form a triple bond; thus, it can have a maximum bond order of three. As the interatomic distance between two carbons increases above 1.2 Å, the pi-pi bond diminishes, the bond order reduces, and a double bond is formed from the triple bond. Similarly, the double bond becomes a single bond above 1.75 Å and fully dissociates above 2.5 Å. The reaxFF parameterization is based on the DFT calculation, and each valence potential parameter is trained to best fit the discrete energy level of chemical configurations undergoing chemical reactions according to the reaction coordinates, as shown in Fig. 8(b) [66].

The most distinguishable application of the RMD simulation from AACMD or CGMD simulations is the degradation involving chemistry. The degradation condition includes harsh service conditions such as hyperthermal bombardment of gaseous molecules as well as continuous exposure to ambient conditions with humidity and oxygen. The thermal decomposition problems have been a representative application of RMD simulations using ReaxFF [67–69]. Typically, two pyrolytic simulations are performed in thermal decomposition study under either aerobic or anaerobic conditions: a cook-off simulation of continuous heating of a periodic polymer unit cell and a stepwise heating simulation of the unit cell. The onset of thermal decomposition and evolution of small molecule reactants according to the system's temperature are analyzed from the cook-off simulation. Reaction scanning is performed from the initial and decomposed molecular structures to study the reaction pathways and the corresponding activation energy in detail. In the stepwise simulation, the reaction rate constant is determined at each temperature from the simulation time-mass change or simulation time-number of unreactive molecules relations. Then, the activation energy of the studied polymer is determined from the simulation temperature-rate constant relationship using the Arrhenius expressions.

While the cook-off simulation externally and intentionally controls the temperature of the system, hyperthermal erosion can mimic pyrolysis and ablation of thermoprotective polymer nanocomposites in space environment by setting up a more realistic description of the harsh environment. For instance, the bombardment of atomic oxygen (AO) is one of the most threatening sources of material degradation in low earth orbit (LEO) environments. To describe the AO bombardment at real aviation speed to the surface of thermoprotective nanocomposites, thin slab models consisting of tested polymers or composites and a finite vacuum for the runway of bombarding oxygen are prepared, as shown in Fig. 9(a) [70]. Owing to the temporal scale limitations, the flux of AO bombarding the surface of nanocomposites is faster than real AO flux in LEO. For the comparative study, however, the flux considered in previous studies enables steady-state temperature evolution and profile, description of small molecule reactants, and surface recession. The representative snapshots of the nanocomposites loaded with polyhedral oligomeric silsesquioxane (POSS) cage, graphene, and CNTs before and after bombarding 175 AO particles are shown in Fig. 9(b) [71]. As the bombardment continues, the surfaces of polyimide (PI) and nanocomposites are eroded, and reactants are desorbed from the surface. Owing to the desorption of reactants, the mass of the original systems decreases, as shown in Fig. 9(c). By embedding POSS, graphene, and CNTs, the surface recession could be effectively mitigated. From the mass loss and the fluence of AO, the erosion yields of the tested materials could be determined; the comparison is shown in Fig. 9(d). Compared with reals Materials International Space Station Experiment (MISSE) results, one order of difference is observed. Nonetheless, the damage mitigation efficacy could be efficiently compared with each other from the ReaxFF RMD simulations.

Another important and unique application of RMD simulation is the environmental aging of polymer and nanocomposites. In hygroscopic and chemical aging, the interaction between water molecules and matrix polymer and oxidative decomposition of the matrix are important chemistries resulting in the degradation of the matrix polymer in composites [72, 73]. While the AACMD simulation study on hygrothermal aging described plasticization and swelling-related degradation, the ReaxFF simulation can further describe the hydrolysis in epoxy resin. Figure 10(a) shows the MD models of cross-linked epoxy-amine network unit cells with different water contents. Applying the accelerated bond boosting method, the hydrolysis process of diglycidyl ether bisphenol A (Bis A)-aromatic amine (DETDA) system including the transition state could be successfully described [Fig. 10(b)]. As the hydrolysis proceeds, an increasing number of water molecules are consumed for the reaction; thus, the number of water molecules in the system decreases as shown in Fig. 10(c). A well-known mechanical degradation of epoxy in hygroscopic aging is plasticization: water contents in epoxy weakens the intermolecular interaction between atoms. According to the ReaxFF simulation, the hydrolysis of the cross-linked network acts as an additional mechanical degradation mechanism. The resultant degradation of Young's modulus of the Bis A-DETDA system is depicted in Fig. 10(d). The ReaxFF simulation can provide a variety of mechanisms that classical MD simulations have not been able to describe and enables an in-depth understanding of the environmental aging of composites.

Concluding Remark and Perspective

In this semi-review, applications of all-atom, coarse-grained, and reactive molecular dynamics simulations for nanocomposites were intensively retraced over the last 20 years.

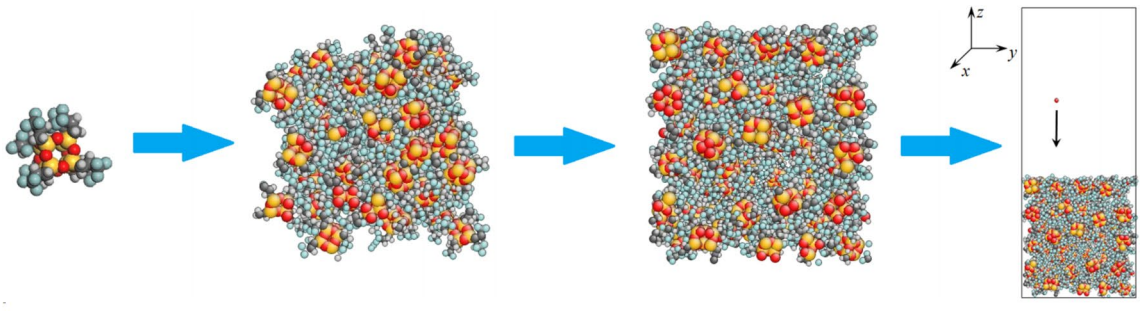

(a)

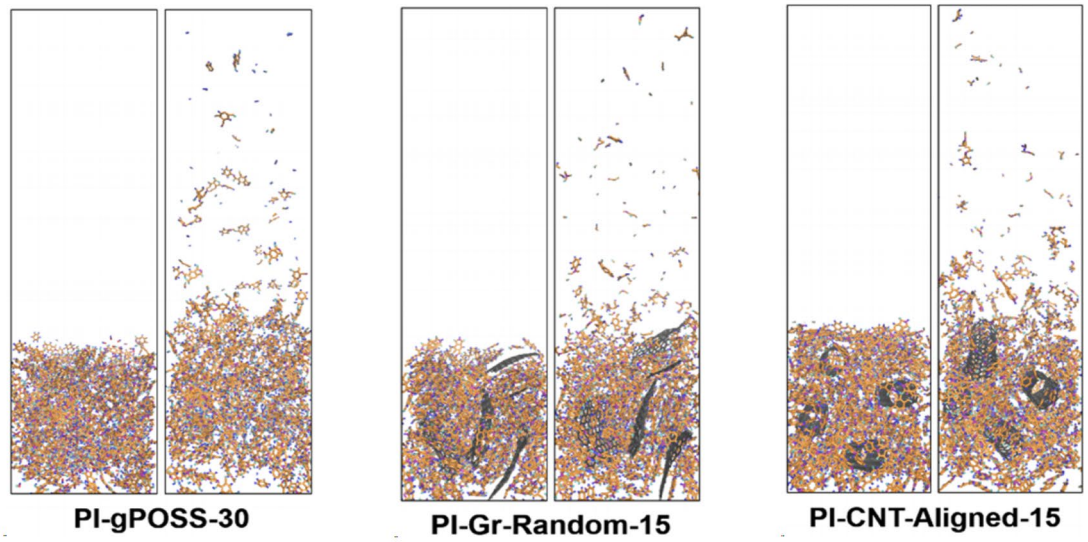

(b)

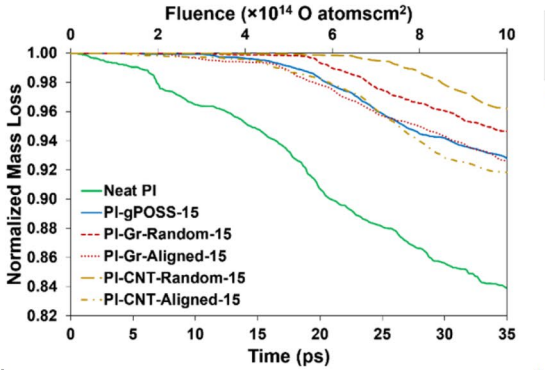

(c)

system	n_{AO} [b]	erosion yield (×10^{-24} g/O atom)				
		13	21	41	72	89
neat PI		4.20	18.32	44.20	79.93	89.90
PI-pPOSS-15		0.00	2.15	5.25	25.00	37.50
PI-pPOSS-30		0.06	0.10	2.02	28.50	29.00
PI-gPOSS-15		0.00	0.72	1.52	5.70	11.60
PI-gPOSS-30		0.00	0.45	0.43	0.31	7.55
PI-Gr-random-15		0.00	0.00	0.06	1.33	1.79
PI-Gr-aligned-15		0.00	0.57	1.83	11.10	16.75
PI-CNT-random-15		0.00	0.00	0.25	0.68	0.56
PI-CNT-aligned-15		0.06	2.55	7.95	9.55	21.50

(d)

Fig. 9 **a** Preparation of the AO bombardment simulation model of 3,3,3-trifluoropropyl POSS [70] (Copyright (2015) American Chemical Society) **b** Representative initial and final snapshots of the PI system after bombarding 50 AO particles. Right: Loaded with 30 grafted POSS nanoparticles, Middle: 15 randomly dispersed graphene flakes. Left: randomly dispersed short SWNTs **c** Time evolution of the normalized mass loss of PI systems loaded with POSS, graphene, and CNTs **d** Average erosion yield at different AO exposures obtained from ReaxFF simulation [71] [Copyright (2017) American Chemical Society]

Undoubtedly, AACMD has successfully contributed to laying the groundwork for establishing the solid theoretical background and structure–property relationship to design multifunctionality. Interface/interphase characterization is still mainstream in the multiscale modeling of nanocomposites. Academically, the interface/interphase of nanocomposites has

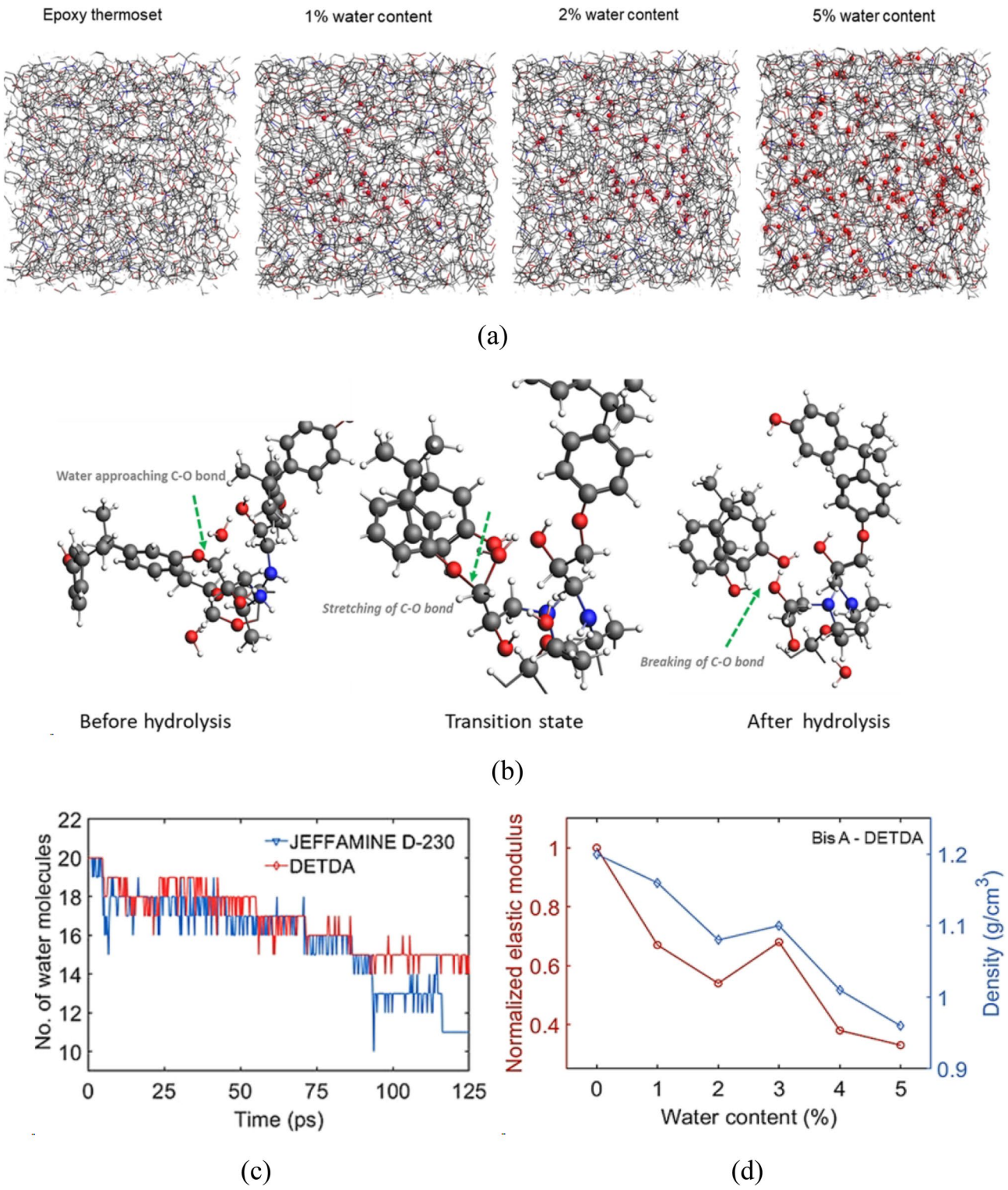

Fig. 10 **a** Cross-lined epoxy periodic unit cell models containing different water contents to study hygroscopic aging (**b**) and epoxy (**c**). The number of water molecules consumed during the hydrolysis reaction of expoy-amine thermosetes **d** Degradation of the elastic modulus of Bis A-DETDA epoxy with varying water content [72] [Copyright (2022) American Chemical Society]

led to the re-examination of mean field micromechanics as a supporting research field. After the solid foundation of in silico simulations accomplished by early-time AACMD, challenges to a more practical and realistic description of the physical behavior of nanocomposites have led to two main streams of CGMD and RMD. CGMD has broadened the temporal and spatial scale of nanocomposite simulations to the micron and submicron levels. Efforts to obtain robust and reliable CG potential parameters are still under progress in computational laboratories to take full advantage of decreasing the degree of freedom in handling various polymer matrices and fillers. Meanwhile, the discovery of unknown phenomena and properties lying between quantum mechanics and classical simulations and new strategies to handle material behavior in digital twin are being continuously attempted.

More than 40 years of development and knowledge of in silico simulation have now standardized the algorithms, numerical recipes, and tricks for the MD simulations. Eventually, both CGMD and RMD are commonly used to develop robust and versatile potential parameters and their validations. Unfortunately, the parameterization of new potential models does not reproduce all the thermoelastic properties due to the state-dependent nature of the ensemble simulations. Nevertheless, some ReaxFF parameters are retrained to improve the accuracy in describing certain special reactions between atoms. Moreover, it is questionable whether temperature transferable CG potentials can guarantee strain rate transferability in describing the mechanical behavior of nanocomposites. Therefore, the future direction of MD potential parameterization will rely on the size of the materials' property database. The recent parameterization process of interatomic potential boosted by machine learning (ML) is a leading breakthrough. To support the ML-assisted parameterization, however, a systematic gathering of materials' properties, construction of an integrated materials' database, and open access to the database should be encouraged systematically.

Acknowledgements The corresponding author Seunghwa Yang greatly appreciate Professor Maenghyo Cho for his encouragement to me and to my excellent lab mates to initiate, to expand and to lead multiscale modeling of polymer nanocomposites.

Funding This work was supported by the National Research Foundation of Korea (NRF) grant funded by the Government of South Korea (MSIT). (No. 2020R1A2C1099749). This paper was supported by the 2022 Innovative Research Program funded by Korea Institute of Civil Engineering and Building Technology.

References

1. P.H.T. Vollenberg, D. Heikens, Particle size dependence of the Young's modulus of filled polymers: 1. Preliminary experiments. Polymer **30**(9), 1656–1662 (1989)
2. P.H.T. Vollenberg, J.W. de Haan, L.J.M. van de Ven, D. Heikens, Particle size dependence of the Young's modulus of filled polymers: 2. Preliminary experiments. Polymer **30**(9), 1663–1668 (1989)
3. S. Iijima, Helical microtubules of graphitic carbon. Nature **354**, 56–58 (1991)
4. P.M. Ajayan, O. Stephan, C. Colliex, D. Trauth, Aligned carbon nanotube arrays formed by cutting a polymer resin-nanotube composite. Science **265**, 1212–1214 (1994)
5. W. Ding, A. Eitan, F.T. Fisher, X. Chen, D.A. Dikin, R. Andrews, L.C. Brinson, L.S. Schadler, R.S. Ruoff, Direct observation of polymer sheathing in carbon nanotube-polycarbonate composites. Nano Lett. **3**(11), 1593–1597 (2003)
6. C. Wei, D. Srivastava, K. Cho, Structural ordering in nanotube polymer composites. Nano Lett. **4**, 1949–1952 (2004)
7. G.M. Odegard, T.C. Clancy, T.S. Gates, Modeling of the mechanical properties of nanoparticle/polymer composites. Polymer **46**(2), 553–562 (2005)
8. S. Yang, M. Cho, Scale bridging method to characterize mechanical properties of nanoparticle/polymer nanocomposites. Appl. Phys. Lett. **93**, 043111 (2008)
9. D. Brown, V. Marcadon, P. Mélé, N.D. Albérola, Effect of filler particle size on the properties of model nanocmposites. Macromolecules **41**, 1499–1511 (2008)
10. L.G. Zhou, S.Q. Shi, Adsorption of foreign atoms on Stone-Wales defects in carbon nanotube. Carbon **41**, 613–615 (2003)
11. J. Gou, Z. Liang, C. Zhang, B. Wang, Computational analysis of effect of single-walled carbon nanotube rope on molecular interaction and load transfer of nanocomposites. Compos. Part B **36**, 524–533 (2005)
12. S.J.V. Frankland, A. Caglar, D.W. Brenner, M. Griebel, Molecular simulation of the influence of chemical cross-links on the shear strength of carbon nanotube-polymer interfaces. J. Phys. Chem. B **106**, 3046–3048 (2002)
13. Q. Zheng, Q. Xue, K. Yan, X. Gao, Q. Li, L. Hao, Effect of chemisorption on the interfacial bonding characteristics of carbon nanotube–polymer composites. Polymer **49**(3), 800–808 (2008)
14. S. Yang, S. Yu, W.M. Kyoung, D.S. Han, M. Cho, Multiscale modeling of size-dependent elastic properties of carbon nanotube/polymer nanocomposites with interfacial imperfections. Polymer **53**, 623–633 (2012)
15. J. Chen, L. Yan, W. Song, D. Xu, Interfacial characteristics of carbon nanotube-polymer composites: a review. Compos. A Appl. Sci. Manuf. **114**, 149–169 (2018)
16. K. Prashantha, J. Soulestin, M.F. Lacrampe, P. Krawczak, G. Dupin, M. Claes, Masterbatch-based multi-walled carbon nanotubes filled polypropylene nanocomposites: assessment of rheological and mechanical properties. Compos. Sci. Technol. **69**, 1756–1763 (2009)
17. L.M. Hamming, R. Qiao, P.B. Messersmith, L.C. Brinson, Effects of dispersion and interfacial modification on the macroscale properties of TiO2 polymer-matrix nanocomposites. Compos. Sci. Technol. **69**, 1880–1886 (2009)
18. D.L. Shi, X.Q. Feng, Y.Y. Huang, K.C. Hwang, H. Gao, The effect of nanotube waviness and agglomeration on the elastic property of carbon nanotube-reinforced composites. J. Eng. Mater. Technol. **126**, 250–257 (2004)
19. H. Shin, K. Baek, J.G. Han, M. Cho, Homogenization analysis of polymeric nanocomposites containing nanoparticulate clusters. Compos. Sci. Technol. **138**(18), 217–224 (2017)
20. J. Liu, Y. Gao, D. Cao, L. Zhang, Z. Guo, Nanoparticle dispersion and aggregation in polymer nanocomposites: insights from molecular dynamics simulation. Langmuir **27**, 7926–7933 (2011)
21. D. Reith, M. Pütz, F. Müller-Plathe, Deriving effective mesoscale potentials from atomistic simulations. J. Comput. Chem. **24**(13), 1624–1636 (2002)

22. M.K. Majumder, S. Ramkumar, D.K. Mahajan, S. Basu, Coarse-graining scheme for simulation uniaxial stress-strain response of glassy polymers through molecular dynamics. Phys. Rev. B **81**, 011803 (2010)
23. H. Park, M. Cho, A multiscale framework for the elasto-plastic constitutive equations of crosslinked epoxy polymers considering the effects of temperature, strain rate, hydrostatic pressure, and crosslinking density. J. Mech. Phys. Solids **142**, 103962 (2020)
24. A.C.T. van Duin, S. Dasgupta, F. Lorant, W.A. Goddard, ReaxFF: a reactive force field for hydrocarbons. J. Phys. Chem. A **105**, 9396–9409 (2001)
25. B. Damirchi, M. Radue, K. Kanhaiya, H. Heinz, G.M. Odegard, A.C.T. van Duin, ReaxFF reactive force field study of polymerization of a polymer matrix in a carbon nanotube-composite system. J. Phys. Chem. C **124**(37), 20488–20497 (2020)
26. J. Hur, Y.N. Abousleiman, K.L. Hull, M.J.A. Qomi, Reactive force fields for modeling oxidative degradation of organic matter in geological formations. RCS Adv. **11**, 29298 (2021)
27. A. Rahnamoun, A.C.T. van Duin, Reactive molecular dynamics simulation on the disintegration of kapton, POSS polyimide, amorphous silica, and teflon during atomic oxygen impact using the reaxFF reactive force-field method. J. Phys. Chem. A **118**, 2780–2887 (2013)
28. C. Wei, Adhesion and reinforcement in carbon nanotube polymer composite. Appl. Phys. Lett. **88**, 093108 (2006)
29. S. Yang, Interface and interphase of nanocomposites tailored by covalent grafting of carbon nanotube: hierarchical multiscale modeling. Int. J. Mech. Sci. **220**, 107160 (2022)
30. S. Yang, S. Yu, J. Ryu, J.M. Cho, W. Kyoung, D.S. Han, M. Cho, Nonlinear multiscale modeling approach to characterize elasto-plastic behavior of CNT/polymer nanocomposites considering the interphase and interfacial imperfection. Int. J. Plast **41**, 124–146 (2013)
31. J.L. Tsai, S.H. Tzeng, Characterizing mechanical properties of particulate nanocomposites using micromechanical approach. J. Compos. Mater. **42**, 2345–2361 (2008)
32. T.C. Clancy, T.S. Gates, Modeling of interfacial modification effects on thermal conductivity of carbon nanotube composites. Polymer **47**, 5990–5996 (2009)
33. V. Varshney, A.K. Roy, J.M. Tyler, J. Lee, B.L. Farmer, Effect of curing and functionalization on the interface thermal conductance in carbon nanotube-epoxy composites. JOM **65**, 140–146 (2013)
34. A.K. Roy, B.L. Farmer, V. Varshney, S. Sihn, J. Lee, S. Ganguli, Importance of interfaces in governing thermal transport in composite materials: modeling and experimental perspectives. ACS Appl. Mater. Interfaces. **4**, 545–563 (2012)
35. S. Yu, S. Yang, M. Cho, Multiscale modeling of cross-linked epoxy nanocomposites to characterize the effect of particle size on thermal conductivity. J. Appl. Phys. **110**, 124302 (2011)
36. M. Hu, P. Keblinski, P.K. Schelling, Kapitza conductance of silicon-amorphous polyethylene interfaces by molecular dynamics simulations. Phys. Rev. B **79**, 104305 (2009)
37. J. Choi, S. Yu, S. Yang, M. Cho, The glass transition and thermoelastic behavior of epoxy-based nanocomposites: a molecular dynamics study. Polymer **52**, 5197–5203 (2011)
38. C. Wei, D. Srivastava, K. Cho, Thermal expansion and diffusion coefficients of carbon nanotube-polymer composites. Nano Lett. **2**(6), 647–650 (2002)
39. F. Pan, F. Peng, Z. Jiang, Diffusion behavior of benzene/cyclohexane molecules in poly(vinylalcohol)-graphite hybrid membranes by molecular dynamics simulation. Chem. Eng. Sci. **62**, 703–710 (2007)
40. C. Wei, Structural phase transition of alkane molecules in nanotube composites. Phys. Rev. B **76**, 134104 (2007)
41. J.S. Yang, C.L. Yang, M.S. Wang, B.D. Chen, X.G. Ma, Crystallization of alkane melts induced by carbon nanotubes and graphene nanosheets: a molecular dynamics simulation study. Phys. Chem. Chem. Phys. **13**, 15476–15482 (2011)
42. S. Yang, M. Cho, A scale-bridging method for nanoparticulate polymer nanocomposites and their nondilute concentration effect. Appl. Phys. Lett. **94**, 223104 (2009)
43. S. Yang, S. Yu, M. Cho, Sequential thermoelastic multiscale analysis of nanoparticulate composites. J. Appl. Phys. **108**, 056102 (2010)
44. J. Choi, S. Yang, S. Yu, H. Shin, M. Cho, Method of scale bridging for thermoelasticity of cross-linked epoxy/SiC nanocomposites at a wide range of temperatures. Polymer **53**(22), 5178–5189 (2012)
45. B. Kim, J. Choi, S. Yang, S. Yu, M. Cho, Influence of crosslink density on the interfacial characteristics of epoxy nanocomposites. Polymer **60**, 186–197 (2015)
46. B. Bhattacharya, Q. Lu, Effect of randomly occurring Stone-Wales defects on mechanical properties of carbon nanotubes using atomistic simulation. Nanotechnology **16**(4), 555–566 (2005)
47. S. Yang, H. Shin, M. Cho, Contribution of oxygen functional groups in graphene to the mechanical and interfacial behaviour of nanocomposites: molecular dynamics and micromechanics study. Int. J. Mech. Sci. **189**(1), 105972 (2021)
48. S. Yang, S. Yu, M. Cho, Influence of Thrower-Stone-Wales defects on the interface properties of carbon nanotube reinforced polypropylene composites by molecular dynamics approach. Carbon **55**, 133–214 (2013)
49. S. Yang, J. Choi, M. Cho, Intrinsic defect-induced tailoring of interfacial shear strength in CNT/polymer nanocomposites. Compos. Struct. **107**, 108–119 (2015)
50. J. Moon, S. Yang, M. Cho, Interfacial strengthening between graphene and polymer through Stone-Thrower-Wales defects: Ab initio and molecular dynamics simulations. Carbon **118**, 66–77 (2017)
51. D. Shin, I. Jeon, S. Yang, Multiscale modeling assessment of the interfacial properties and critical aspect ratio of structurally defected graphene in polymer nanocomposites for defect engineering. Eur. J. Mech.-A/Solids **96**, 104728 (2022)
52. J. Liu, S. Wu, L. Zhang, W. Wang, D. Cao, Molecular dynamics simulation for insight into microscopic mechanism of polymer reinforcement. Phys. Chem. Chem. Phys. **13**, 518–529 (2011)
53. J. Shen, J. Liu, H. Li, Y. Gao, X. Li, Y. Wu, L. Zhang, Molecular dynamics simulations of the structural, mechanical and viscoelastic properties of polymer nanocomposites filled with grafted nanoparticles. Phys. Chem. Chem. Phys. **17**, 7196–7207 (2015)
54. H. Yagyu, T. Utsumi, Coarse-grained molecular dynamics simulation of nanofilled crosslinked rubber. Comput. Mater. Sci. **46**, 286–292 (2009)
55. K. Hagita, H. Morita, M. Doi, H. Takano, Coarse-grained molecular dynamics simulation of filled polymer nanocomposites under uniaxial elongation. Macromolecules **49**, 1972–1983 (2016)
56. S. Park, J. Moon, B. Kim, M. Cho, Multi-scale coarse-grained molecular dynamics simulation to investigate the thermos-mechanical behavior of shape-memory polyurethane copolymers. Polymer **213**, 123228 (2021)
57. R.K. Giri, N. Swaminathan, Role of mapping schemes on dynamical and mechanical properties of coarse-grained models of cis-1, 4-polyisoprene. Comput. Mater. Sci. **208**, 111309 (2022)
58. K. Duan, Y. He, Y. Li, J. Liu, J. Zhang, Y. Hu, R. Lin, X. Wang, W. Deng, L. Li, Machine-learning assisted coarse-grained model for epoxies over wide ranges of temperatures and corss-linking degrees. Mater. Des. **183**, 108130 (2019)
59. D.D. Hsu, W. Xia, S.G. Arturo, S. Keten, Thermomechanically consistent and temperature transferable coarse-graining of atactic polystyrene. Macromolecules **48**, 3057–3068 (2015)

60. C. Wu, R. Wu, W. Xia, L. Tam, Understanding creep behavior of semicrystalline polymer via coarse-grained modeling. J. Polym. Sci. Polym. Phys. **57**, 1779–1791 (2019)
61. V. Agrawal, K. Holzworth, W. Nantasetphong, A.V. Amirkhizi, J. Oswald, S. Nemat-Nasser, J. Polym. Sci. Polym. Phys. **54**, 797–810 (2016)
62. Y. Wang, Z. Meng, Mechanical and viscoelastic properties of wrinkled graphene reinforced polymer nanocomposites-effect of interlayer sliding within graphene sheets. Carbon **177**, 128–137 (2021)
63. J. Yang, D. Custer, C.C. Chiang, X. Meng, X.H. Yao, Understanding the mechanical and viscoelastic properties of graphene reinforced polycarbonate nanocomposites using coarse-grained molecular dynamics simulations. Comput. Mater. Sci. **191**, 110339 (2021)
64. D. Porezag, T. Trauenheim, Th. Kehler, G. Seifert, R. Kaschner, Construction of tight-binding-like potentials on the basis of density-functional theory: application to carbon. Phys. Rev. B **51**(19), 12947–12957 (1995)
65. J. Tersoff, New empirical approach for the structure and energy of covalent systems. Phys. Rev. B **37**(12), 6991–7000 (1988)
66. M. Kowalik, C. Ashraf, B. Damirchi, D. Akbarian, S. Rajabpour, A.C.T. van Duin, Atomistic scale analysis of the carbonization process for C/H/O/N-based polymers with the ReaxFF reactive force field. J. Phys. Chem. B **123**, 5357–5367 (2019)
67. K. Chenoweth, S. Seung, A.C.T. van Duin, W.A. Goddard III., E.M. Kober, Simulations on the thermal decomposition of a poly(dimethylsiloxane) polymer using the ReaxFF reactive force field. J Am. Chem. Soc. **127**, 7192–7202 (2005)
68. Z. Dia, Y. Zho, B. Chen, C. Duan, S. Song, ReaxFF reactive force field for molecular dynamics simulations of epoxy resin thermal decomposition with model compound. J. Anal. Appl. Pyrol. **104**, 618–624 (2013)
69. X. Lu, X. Wang, Q. Li, X. Huang, S. Han, G. Wang, A ReaxFF-based molecular dynamics study of the pyrolysis mechanism of polyimide. Polym. Degrad. Stab. **114**, 72–80 (2015)
70. F. Zeng, C. Peng, Y. Liu, J. Qu, Reactive molecular dynamics simulations on the disintegration of PVDF, VP-POSS, and their composite during atomic oxygen impact. J. Phys. Chem. A **119**, 8359–8368 (2015)
71. F. Rahmani, S. Nouranian, X. Li, A. Al-Ostaz, Reactive molecular simulation of the damage mitigation efficacy of POSS-, graphene-, and carbon nanotube-loaded polyimide coatings exposed to atomic oxygen bombardment. ACS Appl. Mater. Interfaces. **9**, 12802–12811 (2017)
72. A. Karuth, A. Alesadi, A. Vashith, W. Xia, B. Rasulev, Reactive molecular dynamics study of hygrothermal degradation of crosslinked epoxy polymers. ACS Appl. Polym. Maetr. **4**, 4411–4423 (2022)
73. X. Zhang, Y. Wu, H. Wen, G. Hu, Z. Yang, J. Tao, The influence of oxygen on thermal decomposition characteristics of epoxy resins cured by anhydride. Polym. Degrad. Stab. **156**, 125–131 (2018)